Steps on Pt stereodynamically filter sticking of O_2

Kun Cao[a], Richard van Lent[a,b], Aart W. Kleyn[c], Mitsunori Kurahashi[d], and Ludo B. F. Juurlink[a,1]

[a]Catalysis and Surface Chemistry, Leiden Institute of Chemistry, Leiden University, 2300 RA Leiden, The Netherlands; [b]Materials and Surface Science, Dutch Institute for Fundamental Energy Research, 5612 AJ Eindhoven, The Netherlands; [c]Center of Interface Dynamics for Sustainability, Institute of Materials, China Academy of Engineering Physics, Chengdu, Sichuan 610207, China; and [d]Surface Characterization Group, National Institute for Materials Science, Tsukuba, Ibaraki 305-0047, Japan

Edited by Alec M. Wodtke, University of Göttingen, Göttingen, Germany, and accepted by Editorial Board Member A. R. Ravishankara May 8, 2019 (received for review February 16, 2019)

Low coordinated sites on catalytic surfaces often enhance reactivity, but the underlying dynamical processes are poorly understood. Using two independent approaches, we investigate the reactivity of O_2 impinging onto platinum and resolve how step edges on (111) terraces enhance sticking. At low incident energy, the linear dependence on step density, independence of step type, and insensitivity to O_2's molecular alignment show that trapping into a physisorbed state precedes molecular chemisorption and dissociation. At higher impact energies, direct molecular chemisorption occurs in parallel on steps and terraces. While terraces are insensitive to alignment of the molecule within the (111) plane, steps favor molecules impacting with their internuclear axis parallel to the edge. Stereodynamical filtering thus controls sticking and dissociation of O_2 on Pt with a twofold role of steps.

heterogeneous catalysis | reaction dynamics | platinum | oxygen

Platinum is typically used as a catalyst in proton exchange membrane fuel cells (1) and to treat automotive exhaust gases (2). Molecular oxygen's reactions on the surface of platinum are known to be complex (3–5). Besides a physisorbed state, in which the molecule shows rotational and vibrational characteristics very similar to gas-phase O_2 (6–9), there are at least two molecular chemisorbed states. A superoxo species, O_2^-, and a peroxo species, O_2^{2-}, have been identified on large, atomically flat planes of a Pt(111) single-crystal surface (9–12):

$$O_2(g) \rightleftharpoons O_{2,phys} \rightleftharpoons O_{2,chem}^{n-}. \quad [1]$$

The chemisorbed molecular states are precursors to dissociation and to reactions with coadsorbates, e.g., H_{ads}. Dissociation leaves two adsorbed oxygen atoms, O_{ads}, on the surface:

$$O_{2,chem}^{n-} \longrightarrow 2O_{\mathrm{ads}}. \quad [2]$$

Although the dynamics of the initial O_2 (g) adsorption to Pt(111) show parallel characteristics of direct and precursor-mediated processes (13, 14), dissociation does not happen immediately upon O_2 (g) impact. It proceeds via the molecular chemisorbed states (15, 16). For high $O_{2,chem}^{n-}$ coverages, desorption and dissociation are in competition at a surface temperature, T_s, around 150 K. This competition leads to the well-known 0.25 ML O_{ads} limiting coverage when exposing Pt(111) to O_2 (g) under most high-vacuum conditions (17). At low O_{ads} coverages, recombinative desorption occurs at $T_s > 800$ K (12, 18, 19).

In line with early experiments probing adsorption from the background (20), experimental molecular dynamics studies on nanostructured Pt surfaces show that monoatomic steps enhance sticking over a broad range of incident energies (21–23). At low incident energy, it presumably proceeds via the physisorbed molecular state indicated in Eq. **1** (13, 23). For high-impact energies, direct dissociation at steps has been suggested (22). If so, monoatomic steps would provide a shortcut from the initial state of Eq. **1** to the final state of Eq. **2**. Scanning tunneling microscopy and temperature-programmed desorption studies confirm that monoatomic steps are more reactive in dissociating O_2 than (111) terraces (24, 25). However, they cannot resolve dynamical mechanisms.

Theoretical studies discriminate between various molecularly chemisorbed states, both at steps and at terraces (24, 26–28). Calculations of sticking support multiple dynamical processes, but have so far considered only Pt(111) (29, 30). A tight-binding molecular dynamics approach even challenged the interpretation of indirect adsorption via a physisorbed state for that surface (29). Tests of future theoretical dynamics studies that include monoatomic steps thus require more detailed experimental evidence for proposed mechanisms leading to O_2 sticking on Pt.

Recently, studies using curved single-crystal surfaces have unraveled structure dependencies of chemical reactions. In combination with supersonic molecular beam techniques, an outstanding issue regarding the dynamics of Pt-catalyzed H_2 dissociation was resolved (31). In combination with a high-pressure reactor, a curved Pd surface revealed a sensitivity to step type and terrace width in CO oxidation (32). The essential ingredient in these studies is the controlled continuous variation of step density over more than two orders of magnitude on the surface of a single crystal with spatial separation of step types. Fig. 1, *Top* schematically illustrates such a curved single crystal.

A new technique allowing for studies of alignment dependencies in O_2 reactions on surfaces uses state selection using a magnetic hexapole and subsequent steering of the molecule's rotational axis before its impact onto the surface (33, 34). For Pt(111), this technique provided direct evidence that activated adsorption into the chemisorbed superoxo and peroxo states is sensitive to the alignment of O_2's internuclear axis upon impact (35). Molecules aligned parallel to the (111) plane more easily find their way into molecular chemisorbed states than those

Significance

Platinum is widely applied as an oxidation catalyst. The surfaces of metallic catalyst particles are generally composed of atomically flat planes connected by edges. In this paper, we unveil how Pt edges affect O_2 sticking. Opposing types of behaviors are observed for high and low incident energies. The dependencies identify the mechanisms by which O_2 molecules stick, which is the first step in the oxidation reactions.

Author contributions: M.K. and L.B.F.J. designed research; K.C., R.v.L., M.K., and L.B.F.J. performed research; K.C., R.v.L., M.K., and L.B.F.J. analyzed data; and K.C., R.v.L., A.W.K., M.K., and L.B.F.J. wrote the paper.

The authors declare no conflict of interest.

This article is a PNAS Direct Submission. A.M.W. is a guest editor invited by the Editorial Board.

See Commentary on page 13727.

[1]To whom correspondence may be addressed. Email: l.juurlink@chem.leidenuniv.nl.

This article contains supporting information online at www.pnas.org/lookup/suppl/doi:10.1073/pnas.1902846116/-/DCSupplemental.

Published online May 29, 2019.

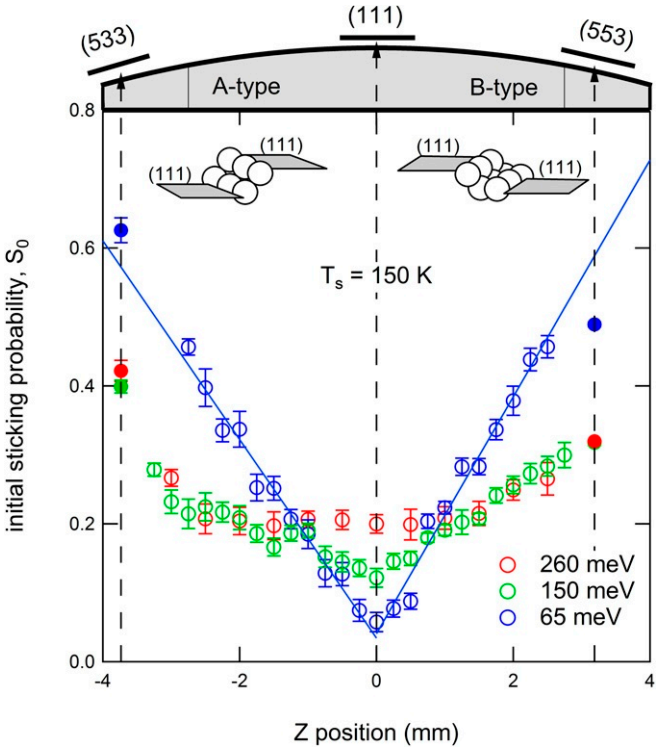

Fig. 1. Initial sticking probability of O_2 as a function of incident position on a curved Pt single crystal for 65 meV, 150 meV, and 260 meV incident energy at T_s = 150 K. Open symbols represent data gathered using the curved single crystal that is schematically represented at *Top* of the graph. Solid symbols were gathered using flat single crystals with (533) and (553) surface structures. Error bars reflect the SD calculated from multiple measurements. *Insets* show the local step structure for the A- and B-type steps.

aligned perpendicular to that plane. This phenomenon was also shown to control CO oxidation kinetics (36).

In this paper, we report how steps on Pt(111) affect the dynamics of O_2 sticking. Combining results from studies using a curved Pt single-crystal surface and studies using the O_2 alignment technique, we unravel contributions from (111) terraces and monoatomic steps to sticking. At low incident energies, sticking is linearly dependent on step density and independent of step type. For two highly corrugated surfaces, we show it is also independent of O_2 alignment. We conclude that for these low-impact energies, steps enhance the initial scattering into a physisorbed state that precedes chemisorption and dissociation. For higher incident energies, direct chemisorption at upper edges is reflected by azimuthal and polar O_2 internuclear alignment dependencies. Our results show that direct processes are step-type dependent.

Results

Fig. 1, *Top* illustrates our curved Pt single crystal. It curves 31° along [11$\bar{2}$] with the apex centered at the (111) plane. The macroscopic curvature is a consequence of a smooth variation in density of monoatomic steps of the A and B types (Fig. 1, *Insets*) (31, 37, 38). These steps expose, respectively, the shortest possible (100) and (110) facets. Their normals are, respectively, rotated by 54.7° and 35.3° in opposite directions from the [111] normal. We probe the O_2 initial sticking probability, S_0, across surface structures from approximately the six-atom wide (111) terraces separated by A-type steps via large and atomically smooth (111) planes at the apex to six-atom wide (111) terraces separated by B-type steps. The molecular beam is incident along the [111] vector. The width of our molecular beam at the crystal is 0.13 mm, approximately equal to the size of the symbols used to indicate data (Fig. 1, open symbols). The probed step density varies, thus, linearly from $\sim$1 nm^{-1} at either edge to less than 10 μm^{-1} at the apex (31). At the indicated surface temperature (T_s = 150 K), the physisorbed state of O_2 is unstable. At the (111) terraces and both step types, O_2 sticks in a chemisorbed state and/or dissociates.

At the lowest incident energy, E_{kin} = 65 meV (blue), sticking is linearly dependent on position, hence step density, on both sides. This can only be accounted for by independent contributions of steps and terraces (31, 39, 40). The solid blue lines in Fig. 1 represent the best fit to the data for the A- and B-type steps. Both fits yield a residual reactivity of 0.04 at the ideal (111) plane. The slopes of the lines are nearly identical, indicating that sticking, as induced by steps at low kinetic energy, is independent of step type.

For reference, solid blue symbols in Fig. 1 indicate data collected under identical conditions using flat single crystals with (533) and (553) surface structures. These surface structures have four-atom wide (111) terraces. Their corresponding locations on the curved crystal surface are indicated by vertical dashed lines. Tapering of the polished surface in this region prohibits measurements using our curved crystal. For B-type steps, extrapolation of the data from the curved crystal yields a slightly higher reactivity than determined here for the (553) surface. Reactivity is rather accurately predicted by extrapolation to (533).

At higher incident energies (green and red in Fig. 1), the reactivity at the (111) apex increases. Simultaneously, the contribution of steps to sticking diminishes quite dramatically. This energy dependence agrees with previous studies for the (111) (13, 14), (533) (22), and (553) (23) surfaces. At 150 meV (green), both sides of the crystal still reflect an approximate linear dependence over a reasonably large step density range. At 260 meV (red), this dependence clearly loses its linear character. Near the apex, reactivity is independent of step density. Near the edges, steps still contribute. Clearly, dynamical processes leading to sticking at higher incident energies are not dominated by steps alone. Direct impingement onto the (111) terraces contributes significantly.

Fig. 2 shows our reference frame and Fig. 3 the results of experiments that probe alignment dependences over a wide kinetic energy range on three flat Pt single crystals. A magnetic hexapole selects a spin-rotational state [(J, M) = (2,2)] of O_2, where the angular momentum vector of body rotation is oriented parallel to the quantization axis (34). Coupling of the magnetic moment of this quantum state to an externally applied magnetic field allows us to steer the rotational axis of the molecule before impact onto a surface. The molecular beam axis lies along the X direction in Fig. 2. We orient the Pt(111), Pt(553), and Pt(533) surfaces such that their (111) facets are normal to the beam propagation axis, hence X. For each crystal, the surface normal makes an angle, α, with the beam propagation axis equal to 0°, 12.3°, and 14.4°, respectively. We have verified by low-energy electron diffraction that the step direction for the nanostructured surfaces is parallel to Z to within a couple of degrees. At first instance, we compare effects resulting from steering of the rotational axis of the impinging O_2 molecules along X, Y, and Z. Relative to the (111) facets, molecules thus exhibit a helicoptering (H) or cartwheeling motion (C_Y, C_Z). A cartwheeling motion is either in plane with the step direction (C_Y) or normal to it (C_Z).

In Fig. 3*A*, we reproduce results published recently for Pt(111) (blue circles) (35). It shows the ratio of the initial sticking probabilities of molecules impinging with a helicoptering motion, $S_0(H)$, and a cartwheeling motion, $S_0(C_z)$, relative to the (111) plane. The data for Pt(111) clearly show that helicoptering molecules stick better than cartwheeling molecules. This is most explicitly observed at low-impact energies, i.e., when

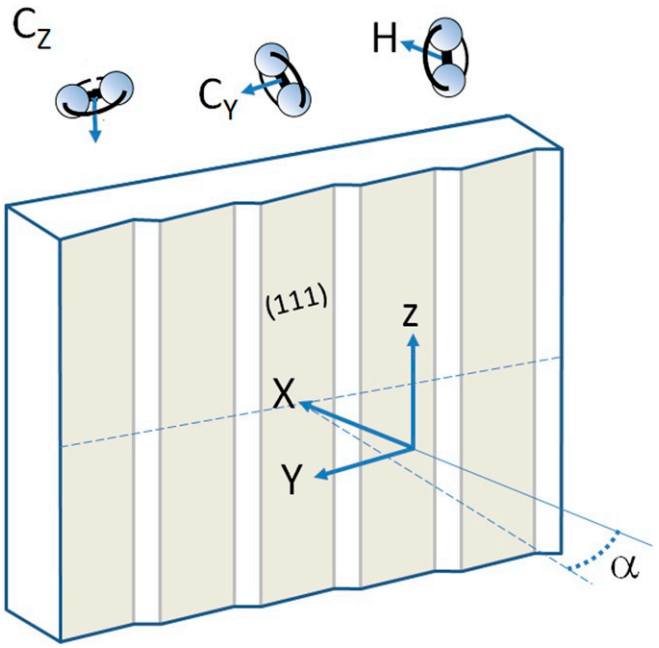

Fig. 2. Directions of rotational motion of O_2 relative to the Pt surfaces. Pt single crystals are oriented such that [111] lies along X. The beam of state-selected O_2 molecules impinges along X. Two thin dashed lines indicate the macroscopic surface normal at an angle α from X and a line along the macroscopic surface in the XY plane. Rotation of state-selected O_2 is aligned with the YZ plane (H), the XZ plane (C_Y), or the XY plane (C_Z).

molecules barely have enough energy to overcome the barrier to direct molecular chemisorption into an $O^{n-}_{2,chem}$ state. This result reflects that molecular chemisorbed states have their O_2 internuclear axis aligned parallel to the surface (35).

The black and red circles in Fig. 3*A* represent additional data for Pt(553) and Pt(533). Clearly, the $S_0(H)/S_0(C_z)$ for both stepped surfaces is drastically different from Pt(111) over a significant part of the energy range. At the lowest kinetic energy the ratio is near unity. The clear favoring of helicoptering molecules in sticking is removed by incorporating either step type at roughly the same step density. With increasing kinetic energy, the alignment preference reappears, though. The data merge with those found for Pt(111) at higher incident energy.

In Fig. 3*B*, we show the ratio $S_0(C_y)/S_0(C_z)$ for both stepped surfaces. These data reflect the alignment dependence of sticking for cartwheeling molecules with respect to the direction of the A- and B-type steps as illustrated in Fig. 2. For both, the ratio varies much less than in Fig. 3*A*, ranging only up to 1.10. Regardless, we observe a clear trend, peaking near 0.2–0.3 eV. Preferential sticking occurs when the rotational plane is along the step direction over the entire energy range. The A-type steps in Pt(533) seem slightly more sensitive to the alignment of J than the B-type steps in Pt(553).

In Fig. 3*C*, we probe a different alignment dependence. Instead of switching between helicoptering and cartwheeling molecules, we arrange the magnetic field such that molecules flip J from +45° (R) to −45° (L) with respect to the molecular beam axis, which is still aligned with X (Fig. 3*C*, *Inset*). For the Pt(111) surface, switching between these R and L rotations has, as expected, no effect. These two states are geometrically equivalent to the (111) surface. For the stepped surfaces, however, a clear deviation is observed. Molecules with the J vector oriented as in R rotate such that the internuclear axis is always roughly parallel to the (100) (or A-type) and (110) (or B-type) step facet. To the facet, the molecule looks like it is, roughly, helicoptering. Rotation as in L combines molecular impact with the internuclear axis being both parallel and orthogonal to the step facet, strongly resembling a cartwheeling motion. Results for A- and B-type steps, as represented by the Pt(533) and Pt(553) surfaces, indicate that both step types clearly favor molecules impacting with their internuclear axis parallel to the step's (100) or (110) facet.

Discussion

The combined results from both types of experiments definitively confirm the hypothesized influence of steps on O_2 sticking at low incident energy. Based on a comparison of the energy dependence for various stepped Pt surfaces, we previously proposed that the dominating contribution to reactivity results from an indirect mechanism that mostly depends on step density—not on step type (23). The strong and linear dependence of sticking on step density at 65 meV in Fig. 1 confirms that sticking is dominated by impact at step sites and indifferent to the exact local arrangement of atoms in the step. The data in Fig. 3*A* add to this conclusion that the mechanism leading to sticking is indifferent to the alignment of O_2 at low energy. Note that the lowest attainable kinetic energy in the alignment study is on the order of 100 meV, where the influence of various types of steps to overall reactivity is already reduced (Fig. 1 and ref. 23). This behavior is characteristic of sticking that proceeds via initial scattering into a physisorbed state (41). As such states are

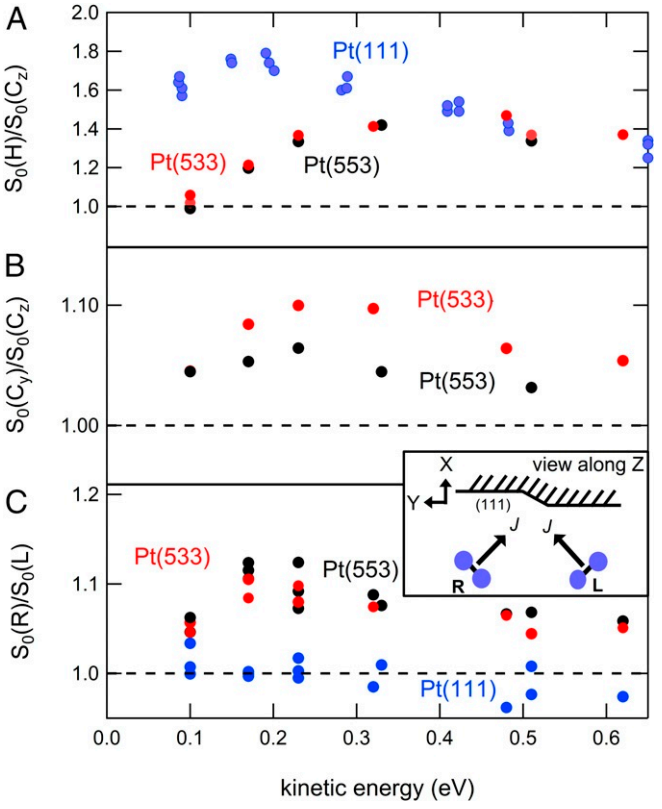

Fig. 3. In *A*, the sticking probability ratios for helicoptering (H) and cartwheeling (C) O_2 molecules on Pt(111) (blue) and Pt(553) (black) are shown as a function of incident energy. In *B* the sticking probability ratios for C_y and C_z for Pt(553) (black) and Pt(533) (red) are shown. *C*, *Upper Inset* depicts the various rotational motions relative to the (stepped) surface. *C* shows the dependence of the step alignment effect for all three surfaces with the same color coding as before for rotations labeled as "R" and "L." The rotational directions in comparison to the (111) facet and line defect directions are illustrated in *C*, *Lower Inset*. The surface temperature for all data shown lies in the range of 300–400 K, ensuring O_2 dissociation.

only weakly bound and resemble the gas-phase species, scattering into the bound state does not depend critically on the alignment of the molecule during the collision. In contrast to chemisorbed states, physisorbed states are also not expected to depend strongly on lateral position. We thus interpret our results as indicative of local geometric corrugation enhancing the probability of redirecting molecules incident along [111] into motion parallel to the (111) plane. Subsequent (dissociative) adsorption may occur there or at a nearby step. Note that this finding is in clear contrast with sticking on Pt(111) at low incident energy. The very low reactivity there (0.04 at the apex in Fig. 1) results predominantly from alignment-sensitive (Fig. 3*A*), direct adsorption into molecular chemisorbed states (35). This mechanism's contribution to the total sticking on highly stepped surfaces can be judged to be more than an order of magnitude smaller than the indirect process proceeding via the physisorbed state in Fig. 1.

Results presented in Figs. 1 and 3*A* also allow us to understand how contributions of various mechanisms for sticking change with increasing kinetic energy. Activated direct adsorption into chemisorbed molecular states on (111) terrace sites increases with kinetic energy. This causes the increase in S_0 at and near the center of the curved crystal in Fig. 1 for 150 meV and 260 meV. The increase is, in part, due to improved sticking of cartwheeling molecules and causes the decreasing ratio $S_0(H)/S_0(C_z)$ in Fig. 3*A* for Pt(111) (35). Simultaneous sticking via initial scattering from steps into a physisorbed state becomes more difficult as a larger velocity vector needs to be redirected. This causes the drop in sticking for stepped surfaces along the curvature of our crystal in Fig. 1. The increasing alignment dependence for the stepped surfaces in Fig. 3*A* reflects the increasing contribution of alignment-sensitive direct adsorption at terraces at the expense of alignment-insensitive scattering into a physisorbed state by steps.

Beyond scattering into the physisorbed state, steps have a second contribution to sticking. This contribution is unveiled by the data in Fig. 3*B*. It shows an alignment dependence, pointing toward direct access of a chemisorbed state at steps. Sticking is favored when the O_2 rotation includes alignment along the step edge. This is consistent with results of a density funtional theory-based study of O_2 molecular binding to various Pt surfaces (24, 28). There, the highest binding energy was found for O_2 bound parallel to the upper edge of the A-type step of Pt(211). The difference with a state parallel to the surface but orthogonal to the step direction was 0.8 eV. The weaker alignment dependence for Pt(553) compared with Pt(533) in Fig. 3*B* may suggest that this difference in binding energy at B-type steps is smaller.

Finally, the data in Fig. 3*C* provide more detail on these molecular states at step edges. The R and L rotations both include molecular alignment along the step edge. Their difference lies in the probed alignment resembling end-on vs. orthogonal π binding relative to the step edge. The preference for helicopter-like rotation relative to the step facet in comparison with cartwheel-like rotation suggests that end-on binding to the step edge is least favorable or even repulsive.

Conclusions

The results of our study show that the influence of steps on alignment dependences in sticking of O_2 is twofold. Through strongly enhancing the scattering probabilities into a physisorbed state at low incident energy, alignment sensitivity to adsorption and dissociation is lost on highly corrugated surfaces. However, with increasing incident energy, direct adsorption into chemisorbed states at edges becomes one of the contributions to overall sticking. This mechanism is alignment dependent and step edges show a clear preference for molecules being aligned parallel to the step. This is a profound observation of a steric effect in a molecule's adsorption at steps.

Materials and Methods

For measurements performed in Leiden, the Netherlands, we used the same supersonic molecular beam apparatus as described in our previous study of O_2 sticking and dissociation on Pt(553) (23). Supersonic expansion of O_2 in various seed gases allows us to vary the incident energy, which we determine by standard time-of-flight (TOF) techniques. In *SI Appendix* we describe our TOF procedures in detail with data presented in *SI Appendix*, Fig. S4 and a typical kinetic energy distribution in *SI Appendix*, Fig. S5. Sticking is measured using the King and Wells approach. Examples are shown in *SI Appendix*, Fig. S3. To attain high local resolution, the molecular beam is skimmed to a rectangular shape with a surface area of 0.13×6.0 mm^2 at the curved crystal's position. The curved crystal is cleaned using a recipe developed before to ensure that step doubling and faceting of less stable surface structures along the curved surface are prevented (31). Stereodynamically sensitive experiments were executed in Tsukuba, Japan, with an apparatus also described before (33, 34). Briefly, supersonically expanded mixtures of O_2 in He pass through a magnetic hexapole containing a variable number of hexapole elements. The number of elements is matched to the kinetic energy of state-selected O_2. Stern–Gerlach (SG) and TOF analyses of O_2 [(J,M) = (2,2)] indicate that the purity of the (J,M) = (2,2) state is nearly 100% and the estimated velocity spread ($\Delta v/v$) is at most 10–15% (33). Three sets of Helmholtz coils are placed on the outside of the ultrahigh vacuum chamber that houses the Pt(553), Pt(533), or Pt(111) crystals upon which the state-selected O_2 molecules impinge. Currents through the Helmholtz coils are alternated every 2 s to switch between two impact geometries for O_2 while sticking is measured using the King and Wells technique. Every experiment using two impact geometries is performed at least twice, also using the reversed order in alternating between impact geometries. Initial sticking probabilities are obtained by extrapolating the best fit of a double-exponential functional form to data over a nearly 60-s time frame to t = 0. *SI Appendix*, Fig. S6 provides an example of a King and Wells trace and the fitting procedure. We use two filters to separately fit results for the two impact geometries. This extrapolation removes various convolutions at the start of the experiment. Reported sticking probabilities are averaged for experiments with the original and reversed orders. Exemplary data and more details on data analysis are provided in *SI Appendix*.

ACKNOWLEDGMENTS. K.C. acknowledges the award of a grant from the Chinese Scholarship Council. L.B.F.J. and M.K. acknowledge funding by the National Institute for Materials Science, Japan. M.K. also acknowledges the support of Japanese Society for the Promotion of Science KAKENHI Grant 16H03874.

1. N. M. Marković, T. J. Schmidt, V. Stamenković, P. N. Ross, Oxygen reduction reaction on Pt and Pt bimetallic surfaces: A selective review. *Fuel Cells* **1**, 105–116 (2001).
2. G. C. Koltsakis, A. M. Stamatelos, Catalytic automotive exhaust aftertreatment. *Prog. Energy Combust. Sci.* **23**, 1–39 (1997).
3. T. Zambelli, J. Barth, J. Wintterlin, G. Ertl, Complex pathways in dissociative adsorption of oxygen on platinum. *Nature* **390**, 495–497 (1997).
4. T. Jacob, The mechanism of forming H2O from H2 and O2 over a Pt catalyst via direct oxygen reduction. *Fuel Cells* **6**, 159–181 (2006).
5. M. M. Montemore, M. A. van Spronsen, R. J. Madix, C. M. Friend, O_2 activation by metal surfaces: Implications for bonding and reactivity on heterogeneous catalysts. *Chem. Rev.* **118**, 2816–2862 (2018).
6. A. C. Luntz, J. Grimblot, D. E. Fowler, Sequential precursors in dissociative chemisorption: O_2 on Pt(111). *Phys. Rev. B* **39**, 12903–12906 (1989).
7. J. Grimblot, A. Luntz, D. Fowler, Low temperature adsorption of O2 on Pt(111). *J. Electron. Spectros. Relat. Phenomena* **52**, 161–174 (1990).
8. W. Wurth *et al*., Bonding, structure, and magnetism of physisorbed and chemisorbed O2 on Pt(111). *Phys. Rev. Lett.* **65**, 2426–2429 (1990).
9. K. Gustafsson, S. Andersson, Infrared spectroscopy of physisorbed and chemisorbed O2 on Pt(111). *J. Chem. Phys.* **120**, 7750–7754 (2004).
10. J. L. Gland, B. A. Sexton, G. B. Fisher, Oxygen interactions with the Pt(111) surface. *Surf. Sci.* **95**, 587–602 (1980).
11. H. Steininger, S. Lehwald, H. Ibach, Adsorption of oxygen on Pt(111). *Surf. Sci.* **123**, 1–17 (1982).
12. N. R. Avery, An EELS and TDS study of molecular oxygen desorption and decomposition on Pt(111). *Chem. Phys. Lett.* **96**, 371–373 (1983).
13. M. D. Williams, D. S. Bethune, A. C. Luntz, Coexistence of precursor and direct dynamics: The sticking of O2 on a Pt(111) surface. *J. Chem. Phys.* **88**, 2843–2845 (1988).
14. A. C. Luntz, M. D. Williams, D. S. Bethune, The sticking of O2 on a Pt(111) surface. *J. Chem. Phys.* **89**, 4381–4395 (1988).

15. C. T. Rettner, C. B. Mullins, Dynamics of the chemisorption of O2 on Pt(111): Dissociation via direct population of a molecularly chemisorbed precursor at high incidence kinetic energy. *J. Chem. Phys.* **94**, 1626–1635 (1991).
16. P. D. Nolan, B. R. Lutz, P. L. Tanaka, J. E. Davis, C. B. Mullins, Molecularly chemisorbed intermediates to oxygen adsorption on Pt(111): A molecular beam and electron energy-loss spectroscopy study. *J. Chem. Phys.* **111**, 3696–3704 (1999).
17. D. L. Bashlakov, L. B. F. Juurlink, M. T. M. Koper, A. I. Yanson, Subsurface oxygen on Pt(111) and its reactivity for CO oxidation. *Catal. Lett.* **142**, 1–6 (2012).
18. J. L. Gland, Molecular and atomic adsorption of oxygen on the Pt(111) and Pt(S)-12(111) $\times$ (111) surfaces. *Surf. Sci.* **93**, 487–514 (1980).
19. S. D. Miller, V. V. Pushkarev, A. J. Gellman, J. R. Kitchin, Simulating temperature programmed desorption of oxygen on Pt(111) using DFT derived coverage dependent desorption barriers. *Top. Catal.* **57**, 106–117 (2014).
20. A. Winkler, X. Guo, H. Siddiqui, P. Hagans, J. Yates, Kinetics and energetics of oxygen adsorption on Pt(111) and Pt(112)- A comparison of flat and stepped surfaces. *Surf. Sci.* **201**, 419–443 (1988).
21. A. V. Walker, B. Klötzer, D. A. King, Dynamics and kinetics of oxygen dissociative adsorption on Pt110(1$\times$2). *J. Chem. Phys.* **109**, 6879–6888 (1998).
22. A. T. Gee, B. E. Hayden, The dynamics of O2 adsorption on Pt(533): Step mediated molecular chemisorption and dissociation. *J. Chem. Phys.* **113**, 10333–10343 (2000).
23. L. Jacobse, A. den Dunnen, L. B. F. Juurlink, The molecular dynamics of adsorption and dissociation of O2 on Pt(553). *J. Chem. Phys.* **143**, 014703 (2015).
24. P. Gambardella *et al*., Oxygen dissociation at Pt steps. *Phys. Rev. Lett.* **87**, 056103 (2001).
25. C. Badan *et al*., Step-type selective oxidation of platinum surfaces. *J. Phys. Chem. C* **120**, 22927–22935 (2016).
26. A. Eichler, J. Hafner, Molecular precursors in the dissociative adsorption of O2 on Pt(111). *Phys. Rev. Lett.* **79**, 4481–4484 (1997).
27. J. S. McEwen, J. M. Bray, C. Wu, W. F. Schneider, How low can you go? Minimum energy pathways for O2 dissociation on Pt(111). *Phys. Chem. Chem. Phys.* **14**, 16677–16685 (2012).
28. Ž. Šljivančanin, B. Hammer, Oxygen dissociation at close-packed Pt terraces, Pt steps, and Ag-covered Pt steps studied with density functional theory. *Surf. Sci.* **515**, 235–244 (2002).
29. A. Gross, A. Eichler, J. Hafner, M. Mehl, D. Papaconstantopoulos, Unified picture of the molecular adsorption process: O2/Pt(111). *Surf. Sci.* **539**, L542–L548 (2003).
30. P. Valentini, T. E. Schwartzentruber, I. Cozmutax, Molecular dynamics simulation of O2 sticking on Pt(111) using the ab initio based ReaxFF reactive force field. *J. Chem. Phys.* **133**, 084703 (2010).
31. R. van Lent *et al*., Site-specific reactivity of molecules with surface defects—The case of H2 dissociation on Pt. *Science* **363**, 155–157 (2019).
32. S. Blomberg *et al*., Strain dependent light-off temperature in catalysis revealed by planar laser-induced fluorescence. *ACS Catal.* **7**, 110–114 (2017).
33. M. Kurahashi, Y. Yamauchi, Production of a single spin-rotational state [(J,M)=(2,2)] selected molecular oxygen ($^3\Sigma_g^-$) beam by a hexapole magnet. *Rev. Sci. Instrum.* **80**, 083103 (2009).
34. M. Kurahashi, Oxygen adsorption on surfaces studied by a spin- and alignment-controlled O2 beam. *Progr. Surf. Sci.* **91**, 29–55 (2016).
35. H. Ueta, M. Kurahashi, Dynamics of O2 chemisorption on a flat platinum surface probed by an alignment-controlled O2 beam. *Angew. Chem. Int. Ed.* **56**, 4174–4177 (2017).
36. H. Ueta, M. Kurahashi, Steric effect in CO oxidation on Pt(111). *J. Chem. Phys.* **147**, 194705 (2017).
37. A. L. Walter *et al*., X-ray photoemission analysis of clean and carbon monoxide-chemisorbed platinum(111) stepped surfaces using a curved crystal. *Nat. Commun.* **6**, 1–7 (2015).
38. A. J. Walsh *et al*., Step-type and step-density influences on CO adsorption probed by reflection absorption infrared spectroscopy using a curved Pt(111) surface. *J. Vac. Sci. Technol. A* **35**, 03E102 (2017).
39. I. M. N. Groot, K. J. P. Schouten, A. W. Kleyn, L. B. F. Juurlink, Dynamics of hydrogen dissociation on stepped platinum. *J. Chem. Phys.* **129**, 224707 (2008).
40. I. M. N. Groot, A. W. Kleyn, L. B. F. Juurlink, The energy dependence of the ratio of step and terrace reactivity for H2 dissociation on stepped platinum. *Angew. Chem. Int. Ed.* **50**, 5174–5177 (2011).
41. M. Kurahashi, Y. Yamauchi, Huge steric effects in surface oxidation of Si(100). *Phys. Rev. B* **85**, 161302 (2012).